Fourier Analysis of Phase Resetting Curves of Neural Oscillators

Robert A. Raidt and Dr. Sorinel A. Oprisan

Department of Physics and Astronomy, College of Charleston, Charleston SC 29424

We investigated the impact of changes in biologically relevant control parameters, such as the shape of an external perturbation or the conductance values of an individual model neuron, on the shape of the phase resetting curve (PRC) of that neuron. For that purpose, PRCs were generated for groups of Morris-Lecar (ML) model neurons with different conductance values but similar firing periods (within 0.005ms) using external rectangular, triangular, or trapezoidal perturbations of varying areas. These PRCs were numerically described and analyzed as a series of coefficient values using a Fourier Discrete Sine Transform (DST). We found that changes in the shape of the external perturbation had no significant impact on the PRC, as long as the overall area of the perturbation remained constant. We also determined that changes in conductance values had a small impact on the overall area of the PRC, however the overall PRC shapes remained similar.

Introduction

The human nervous system is comprised of tens of thousands of neurons, which transmit and process information using electrical impulses that travel across their membranes. Neurons form specialized neural networks dedicated to different functions, such as sensing, formatting, transmitting and processing visual or auditory stimuli [5]. Some neural network contain relatively few cells, like the spinal reflex networks, and others contain tens of thousands of cells, like the auditory neural networks located in the auditory cortex of the temporal lobe [5].

Neurons generate and transmit electrical impulses through manipulations of the electrochemical gradients established across the cell membrane, which is very permeable to potassium (K^+) and slightly permeable to sodium (Na^+) ions [4]. Usually, the extracellular medium contains a high concentration of Na^+ ions (≈440mM/L) compared to intracellular medium (≈60mM/L). For K^+ ions the concentrations are opposed to Na^+, i.e., the intracellular compartment contains a high concentration of K^+ ions (≈400mM/L) compared to extracellular medium (≈20mM/L). These ions can move across the cell membranes through watery pores called ion channels [2,6,14]. Because of Na^+ concentration alone, the interior of the cell has a positive potential with respect to extracellular medium, which is called Nernst (electrochemical) potential and is about E_{Na} = +50mV [2,4]. Similarly, due to K^+ concentration gradient its Nernst potential is E_K = -90mV, i.e., the interior of the cell has a negative electric potential with respect to extracellular medium. Since cell membranes have both sodium and potassium channels, the electrical potential of the cell settles at about -65mV, which is in between the Nernst potentials of Na^+ and K^+ ions and closer to E_K since the membrane is more permeable to potassium [5]. At rest, both K^+ and Na^+ ions constantly flow out/into the cell down their electrochemical gradient. In order to maintain a stable concentration gradient across the membrane, the Na^+/K^+-ATP pump constantly moves $3Na^+$ ions outside the cells and brings $2K^+$ ions in during every pump cycle.

In addition to the above "general purpose" Na^+ and K^+ channels that are open all the time and contribute to resting membrane potential, called leak channels, there are many other specialized ionic channels [2,5,6,14]. These ion channels are integral membrane proteins that can change their conformation in response to electric pulses and allow ions to enter or exit a cell. There are many types of ion channels that respond to various stimuli, such as pressure-sensitive which respond to mechanical stimuli [2] or ligand gated that respond to specific extracellular ligand molecules [14], however voltage gated ion channels open in response to a change in the electrochemical gradient across the cell membrane [5].

Excitable cells, such as neurons and cardiac cells, communicate with each other through brief electrical signals called action potentials (AP), which are brief bursts of electrical activity that bring the membrane from rest (-65mV) to about +40mV over a few milliseconds. APs are produced and shaped by voltage sensitive ion channels. Initially, in response to an outside excitation (depolarization), a few voltage-gated Na^+ channels open quickly allowing Na^+ ions to enter the cell and further depolarize it. As a result, more Na^+ channels open, which in turn further depolarizes the cell, until it crosses the firing threshold and generates an AP. After 1-3ms of constant depolarization, Na^+ channels inactivate, i.e., close and enter a refractory period during which further membrane depolarization cannot reopen them [1,3,5]. The inactivation of Na^+ channels limits the depolarization overshoot to about +40mV. In addition, a prolonged (1-3 ms) depolarization slowly opens voltage-gated K^+ channels. As a result, K^+ ions flow out of the cell and drive down (repolarize) the membrane to its resting value of -65V. As opposed to Na^+, voltage-gated K^+ ion channels never inactivate. Although the above-described mechanism is the foundation of any so-called conductance-based model of excitable cells, in reality there are many more ionic species involved in generating an AP, e.g., calcium, chlorine, magnesium, etc. Furthermore, each ionic species has multiple ion channel (proteins) types that can actively transport them across the membrane [2,5,6,14]. For example, there are over twenty different types of K^+ channels, some of them do not inactivate (as above), some

inactivate (like Na^+ channels), some require Ca^{2+} presence to function, etc.

Hodgkin and Huxley [4] showed experimentally that, despite the wide variety of morphologies, ion channel types, and AP shapes, there are only two classes of excitable cells that produce oscillatory activities. Type I excitability class refers to neurons that can fire an AP of arbitrarily low frequency in response to an externally injected bias current, whereas type II neurons can only oscillate above a critical frequency [1,3,4]. Most neurons are intrinsic oscillators with a specific intrinsic period P_i, which is the time interval between two successive crossings of an arbitrary membrane voltage threshold in the same direction.

The phase resetting curve (PRC) theory reduce the complexity of the ionic mechanisms involved in generating APs to measuring the response of the neurons to a brief perturbation applied at different phases during a cycle of activity [10,15,18]. The PRC is a graphical representation of the advances or delays of the subsequent spike produced by a perturbation, e.g., a presynaptic input from another neuron [1,3,9,10,15].

The ultimate goal of neuroscience is to understand how the brain works, but to achieve this goal there is no unique pathway. In some cases, e.g., when designing a new and very specific drug targeting a neurodegenerative disease, it is important to capture in a mathematical model all details of a neuron from the very detailed description of every single ion channel up to the morphology of the cell [2,6,14,18]. In other cases, e.g., when understanding the principles of organization and the functions of neural networks, a rudimentary description of a neuron suffices [1,8]. The PRC method is part of the approaches available for investigating the mechanisms that lead to network functions and how they evolve, e.g., during the transition from normal brain activity to epileptic seizure, etc.

The fundamental assumption in using the PRC as a tool for predicting synchrony (epileptic seizures) [9,11] or phase-locked modes (gait patterns and normal brain rhythms) [10,12,13] in coupled neural networks is that the transient PRC measured for isolated neurons (open-loop) remains the same under the recurrent inputs of a phase-locked mode (close-loop). If a stable oscillatory neural activity exists, then a phase variable could be unambiguously defined as the normalized stimulus time with respect to the intrinsic period of oscillation [1,3,15,17]. By convention, the first order transient phase change is defined by (see Fig. 1) [10,13]:

$$F^1(\varphi) = F^1(t_s/P_i) = P_1/P_i - 1, \quad (1)$$

and measures the relative advance or delay of the subsequent spike induced by an incoming input at phase $\varphi = t_s/P_i$. Higher order PRCs can be defined similarly. Alternatively, resetting induced by an incoming stimulus could be tabulated in terms of the neural oscillator's response (or recovery) time in open loop – the stimulus time resetting curve (STRC) [9,12]:

$$t_r = f(t_s). \quad (2)$$

Figure 1 shows how the intrinsic period, P_i, of a neural oscillator is impacted by an external, inhibitory perturbation (vertical arrow), causing new firing periods of P_1; P_2; etc. The plot of the phase change, $P_1/P_i - 1$, as a function of the stimulus phase, $\varphi = t_s/P_i$, gives the PRC (see Fig. 3).

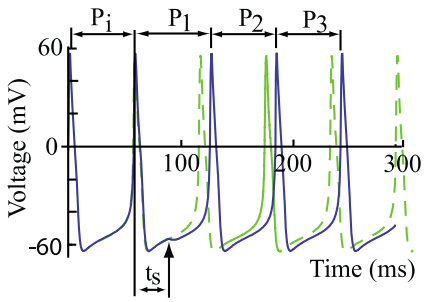

Figure 1. An oscillating Type I neuron experiencing an external, inhibitory perturbation (vertical arrow at stimulus time t_s). The unperturbed (dashed line) trace with intrinsic period P_i suffers a transient change in the firing period (continuous trace).

The advantage of the PRC method is that it allows theoretical predictions regarding the existence and stability of phase-locked modes starting from known differential or difference equations for model neurons [1,3,14]. In contrast, our prediction of phase-locked modes and the analysis of their stability does not assume any knowledge of the system equations, but rather use the PRCs that can readily be generated experimentally in any electrophysiology lab [10,12,13]. In addition, our prediction method relaxed some restrictive assumptions commonly used in proofs regarding phase-locked modes such as weak coupling requirement (see [13] for a review). The first step in our PRC-based prediction of phase-locked firing patter is the computation of the open-loop PRC, i.e., the model neuron is treated as a black box which receives a single external electrical input and produces a transiently modified firing pattern that encodes that input. We showed that this method accurately predicts 1:1 phase locked behavior in Type I neurons, where two oscillating neurons are coupled to each other and impact the others firing patterns [10,12]. Type I and Type II neurons exhibit very predictable behavior in both open loop and 1:1 phase locked models. When exposed to an excitatory presynaptic input, Type I neurons only advance in phase, whereas Type II neurons will experience both advance and delay of phase, depending on the stimulus phase [1,3,15]. Furthermore, Type I neurons have been shown to have a linear region where, in weakly coupled neurons, the transient change in firing rate is proportional to the net presynaptic input [12].

Methods

Morris-Lecar Model

All conductance-based models of excitable cells can be reduced to equivalence electrical circuits, which represent the various electrochemical processes that contribute to APs [1,4,5]. Although no mathematical model is completely accurate biologically, they are useful conceptual tools. Ion channels are represented as electric resistors coupled with a battery, and the cell membrane is represented as a capacitor [1,4,5]. The equivalence electrical circuit of an excitable cell is an extremely versatile model, as many other processes, such as active ion pumps, can be included with relative ease (see

Fig. 2). Morris-Lecar (ML) model was originally developed to mathematically replicate the calcium and potassium-driven oscillations that occur in the muscle fiber of a giant barnacle [1,8]. Therefore sodium ions, which are one of the primary ions involved in mammalian neurons [5], are not considered in this model. Figure 2 shows the equivalent electrical circuit of a ML model neuron for which Kirchhoff's rules give us [1,8]:

$$\sum I = 0 \quad \Leftrightarrow \quad C_M\, dV/dt + I_{Ca} + I_K + I_L + I_{bias} = 0, \qquad (3)$$

which states that the sum of the capacitive current, $I_C = C_M\, dV/dt$, calcium, I_{Ca}, potassium, I_K, leak, I_L, and bias, I_{bias}, currents equals zero (see Fig. 2).

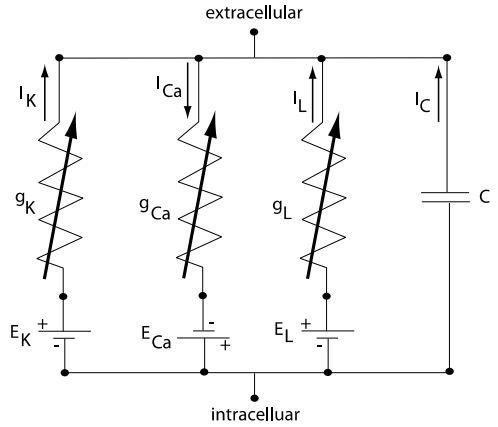

Figure 2. The equivalent electrical circuit of Morris-Lecar model. The three resistor and battery pairs represent the calcium, I_{Ca}, potassium, I_K, and leak, I_L, currents, while the capacitor represents the equivalent membrane capacitance of the neuron.

According to Hodgkin and Huxley paradigm, all ionic currents are usually described by Ohm's law [4,5,8]:

$$I = \Delta V/R = g\,(V - E), \qquad (4)$$

where V is the membrane potential, E is the reverse (Nernst) electrochemical potential of a specific ion channel, and g is the specific conductance (inverse of electrical resistance) value of the ion channel. In the most simplified representation of ionic channels, they cycle through three possible states: open (allow ions to flow), closed (no ions flow), and inactive (recovering from close state and ready to open again) [2,5,6,14]. In general, the conductance g is voltage-dependent and is often written as $g = g_X\, m^p h^q$ where g_X is the (constant) maximum conductance of the respective ionic channel, i.e., assuming that all available channels are open, $m = m(V)$ is the activation function and represents the percentage of the respective ionic channels open at a given membrane potential voltage V, p is a constant exponent, $h = h(V)$ is the inactivation function and represents the percentage of the respective ionic channels inactive at a given membrane potential voltage V, and q is a constant exponent [1,4,5,15,17]. Both the activation and inactivation variables are time and voltage-dependent and, in the simplest scenario, they are described by first order kinetics [1,4,5,15,17]: $dx/dt = (x_\infty - x)/\tau_x$, where $x_\infty = x_\infty(V)$ is the steady-state activation or inactivation of the respective ionic channels and represents the fraction of channels open at a given voltage V, $\tau_x = \tau_x(V)$ is the characteristic time constant of the respective ionic channels. Usually, the steady-state activations/inactivation functions $x_\infty(V)$, or the gating variables, are mathematically described by sigmoidal functions and the characteristic time $\tau_x(V)$ by Gaussian or a double exponential curves (see below).

By combining (3) and (4), we get the explicit model equations for a ML model neuron:

$$\begin{aligned} C_M\, dV/dt &= -\, g_{Ca}\, m_\infty\, (V - E_{Ca}) - g_K\, w\, (V - E_K) \\ &\quad - g_L\, (V - E_L) - I_{bias}, \\ dw/dt &= \phi\, (w_\infty - w)/\tau_w, \end{aligned} \qquad (5)$$

where w represents the fraction of K^+ ionic channels open at any given time, $m_\infty = .5(1 + \tanh((V\text{-}V_1)/V_2))$ is the activation function of Ca^{2+} ionic channels and represents the fraction of channels open at a given voltage V, $w_\infty = .5(1 + \tanh((V\text{-}V_3)/V_4))$ is the activation function of K^+ and represents the fraction of channels open at a given voltage V, and the characteristic time constant of K^+ channels is $\tau_w = 1/\cosh((V\text{-}V_3)/2V_4))$. In this model, neither Ca^{2+} nor K^+ channels inactivate. The leak current is pure Ohmic, i.e., its conductance is constant. The parameter values for a Type II excitable cell are: $V_1 = -0.01$; $V_2 = 0.15$; $V_3 = 0.0$; $V_4 = 0.3$; $V_{Ca} = 1$; $V_K = -0.7$; $V_L = -0.5$; $C_M = 1$; $\phi = 0.2$, and $I_{bias} = 0.45$ [1]. These are dimensionless (normalized) voltages measured with respect to the calcium reversal potential of E_{Ca}=120 mV. The values for g_K and g_L normalized with respect to g_{Ca} = 4 mS/cm^2 (see Table 1).

PRC Generation

All numerical simulations were run on Mathematica version 8. A computer program was written, incorporating the equations of the ML model (5), which simulated the firing of a Type II spiking neuron being injected with a constant bias current. The intrinsic period, P_i, of the oscillating neuron was calculated by recording the time between multiple positive crossings of a specific threshold. In some cases, the bias current was not able to sustain steady oscillations. Although an arbitrary criterion, we discarded all data if the model did not produce stable oscillations for at least 100 ms (about seven stable spikes - see Table 1) above the threshold.

An external perturbation was then simulated by adding a time-dependent rectangular current pulse to the first (voltage) equation (5) with the desired duration and amplitude. The duration of the perturbation was 5% of the intrinsic period, P_i, and the amplitude was a percentage of the bias current. The subsequent positive crossing of the previously defined threshold was recorded, which allowed P_1 to be determined, from which the PRC was computed according to (1).

A total of 300 stimulus phases were calculated at equal intervals, ranging from 0% to 99.67% of the intrinsic period, to create each PRC. The PRC was then discrete sine transformed (DST). An inverse DST was subsequently performed to check the accuracy of the DST.

Discrete Sine Transform and Analysis

In order to describe and quantify the differences in shape and characteristics between multiple PRCs, a DST was performed on all PRCs generated. The DST is a specific type of Fourier transform that describes a periodic curve as a series of

coefficients that relate to individual sine curves. These coefficients X_s are calculated by applying the equation [7,16]:

$$X_s = \sum_{r=1}^{n} u_r \sin(\pi/n(r-1/2)(s+1)/\sqrt{n}, \quad (6)$$

to a list u_r, i.e., the PRC, of discrete length n. An inverse DST can then be performed to recover the shape of the PRC based on the DST coefficient values. The DST has the potential to generate hundreds of coefficients for an individual curve. However, due to data storage and processing limitations, only the first twenty coefficients generated were stored and analyzed (see Fig. 3).

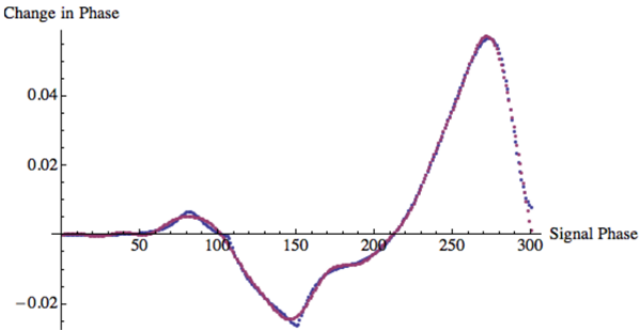

Figure 3. PRC generated by ML model neuron (blue) overlaid with a PRC calculated from an inverse DST of the first twenty coefficients. The PRC curve generated through inverse DST from twenty coefficients recreates the PRC much more accurately than by using only ten coefficients (not shown).

While removing the higher order coefficients from the analysis does introduce some error to the results, these coefficients only cause small changes to the overall shape of the recreated PRC, so any errors can be assumed to be negligible.

By describing a PRC as a series of DST coefficients, comparing similarities between a group of individual curves becomes a matter of comparing the deviations between each of the n^{th} order coefficients for all the curves being compared. This analysis was limited to coefficients that relate to sine functions, therefore the first DST coefficient was not analyzed, as it is a measure of overall amplitude and does not relate to a sine curve. Using this Fourier analysis, a set of coefficients was determined to have a significant deviation if the standard deviation of the set was greater than 50% of the average value of all the DST coefficients of that set. This deviation could be caused by a systemic deviation of multiple DST coefficients or a single outlier lying far from the mean, however both causes of deviation were treated the same and both lead to that set being labeled as deviating significantly for further analysis.

Experimental Procedure

Gene mutations causing changes in the ion flux of voltage gated ion channels have been associated with various neurological diseases such as epilepsy [2,5,6,18], so analyzing how such changes in ion channel conductance impacts the PRC can offer insight into the mechanisms which cause these diseases. Also, changes in external perturbation shape can demonstrate how various forms of presynaptic input can impact the firing patterns of an individual neuron involved in a larger network.

To be able to predict the firing patterns of large neural networks using PRCs, it is first necessary to understand how changes in biologically relevant control parameters impact the shape and characteristics of the PRC of that neuron. To that affect, two specific parameters were examined: 1) the values of individual ion channel conductance with a fixed rectangular shape of the stimulus, and 2) and variable shape of the external perturbation used to generate the PRC.

To examine the potential impact of ion channel conductance values on the overall shape of the PRC, three groups of neurons were analyzed (see subsection 1. Rectangular Perturbations and Variable Conductances of the Results section). Each group had one conductance value held constant while the other two were manipulated, resulting in either five or six neurons with similar firing periods, within 0.005 milliseconds (see Fig. 4). Each group was named using the conductance value being held constant, i.e., g_{Ca} constant, g_K constant, and g_L constant, and each set of conductance values was assigned an individual name for later graphical analysis (see Table 1 for the parameter values for each neuron of each group).

Neuron #	Period (ms)	g_{Ca}	g_K	g_L
1	13.1611	1.0067	1.9867	.5
2	13.1588	1.02	2.0067	.5
3	13.1571	1.0333	2.0267	.5
4	13.1559	1.0467	2.0467	.5
5	13.1553	1.06	2.0667	.5
6	13.1552	1.0733	2.0867	.5
1	13.9129	1.08	2	.536
2	13.9084	1.0867	2	.548
3	13.9069	1.0933	2	.56
4	13.9084	1.1	2	.572
5	13.9127	1.1067	2	.584
1	14.0647	1.1	2.0867	.458
2	14.0597	1.1	2.06	.488
3	14.0646	1.1	2.033	.518
4	14.0561	1.1	2.0133	.542
5	14.0557	1.1	1.9933	.566

Table 1. Values used for the calcium, potassium, and leak conductances for each model neuron analyzed and the associated periods. Individual labels are given to all neurons in each set for use in graphical analysis. All neuron names have been given in terms of increasing or decreasing values for the two conductances being manipulated.

To analyze the impact that the shape of the external perturbation had on the overall shape of the PRC three different perturbation shapes were used to generate a PRC for a model neuron; a rectangular pulse, a triangular pulse, and a trapezoidal pulse with equal durations for rise, run, and fall (see the subsection 2. Variable Perturbation Shape of the Results section). All pulses lasted for 5% of the intrinsic period, P_i, and the area for each pulse was held constant for all perturbations by manipulating the amplitude (see Fig. 6).

PRCs were generated for each neuron using rectangular, trapezoidal, and triangular pulses lasting 5% of the intrinsic period with amplitudes of 10% and 20% of the bias current. This was done in order to increase the number of samples that could be used for comparison. All PRCs were then stored as a list of twenty DST coefficients and the results were all compiled into groups based on the perturbation and which conductance value was held constant. This resulted in a total of 342 sets of DST coefficients to be analyzed for any significant deviations (see Fig. 6).

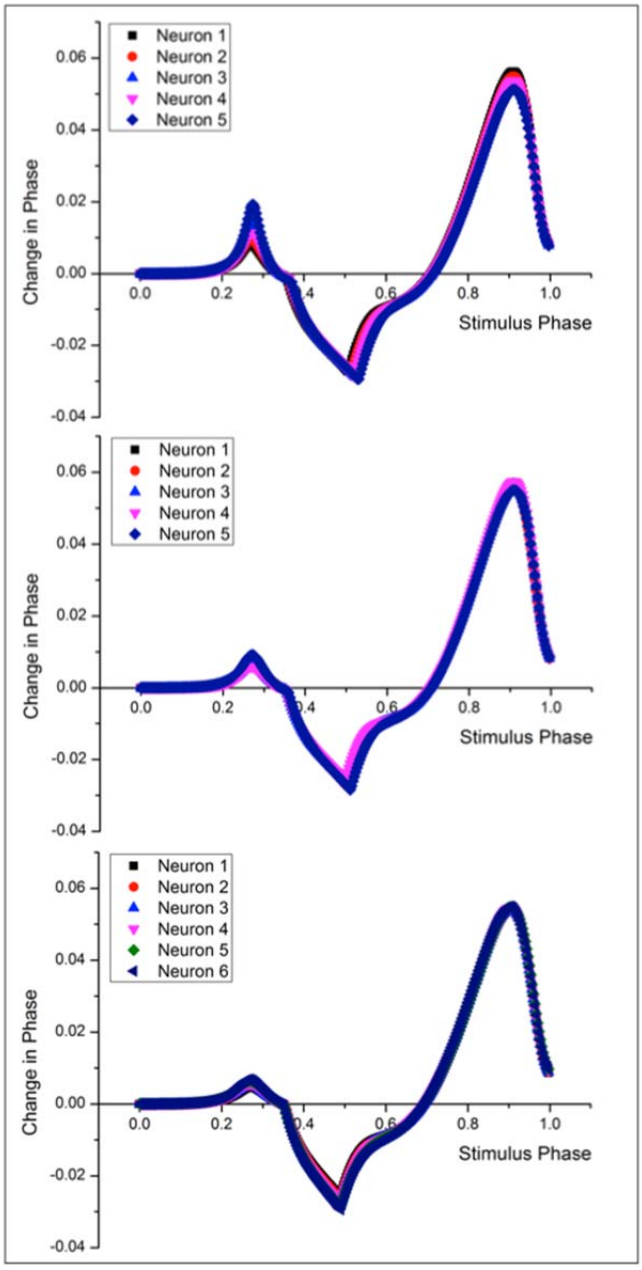

Figure 4. All PRCs generated with a 20% rectangular pulse holding g_{Ca} constant (top), g_K constant (middle), or g_L constant (bottom), suggests that overall PRC shape remained relatively unchanged while changing individual conductance values.

Results

1. Rectangular Perturbations and Variable Conductances

When individual conductance values were changed while maintaining the same period, the overall shape of the PRC did not significantly change. In total 20% of the 342 sets of DST coefficients were found to contain significant deviations, while 80% of all the coefficients generated remained similar. This is shown in Figure 4, which contains PRCs generated from each of the three groups with a 20% rectangular pulse. The significant overlap of the PRCs in each group shows that the overall shape of the PRCs remain similar for each neuron.

However, an unexpected trend was noted between the individual conductance values and the areas of the advancing and delaying sections of the PRC. Figure 5, which overlays multiple PRCs generated with a 20% rectangular pulse keeping g_{Ca} constant, shows how g_K and g_L relate to the areas of the advancing and delaying sections. As g_L increases, the area of the advancing section increases while the area of the delaying section decreases. Conversely, increasing g_K decreased the area of the advancing section while increasing the area of the delaying section. Increases in g_{Ca}, which are not shown in Figure 5, act similar to increases in g_L, where the advancing area increases and the delaying area decreases. Although this trend occurred throughout all trials performed, the overall change in area was relatively small, the largest of which being a 6% deviation from the mean area of the trial.

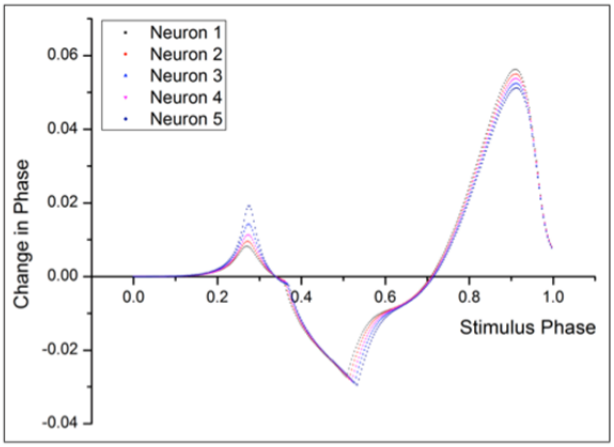

Figure 5. PRCs generated using a 20% rectangular pulse holding g_{Ca} constant with smaller data points, showing the drifts in advancing and delaying area associated with increasing or decreasing conductance values.

These trends did not always correlate to increases or decreases in the intrinsic period of the neurons. When g_L was held constant, increases in g_{Ca} and g_K correlated with a decrease in period, however when g_K and g_L were held constant period did not increase or decrease in relation to either coefficient. Also, when g_L was held constant, the advancing area remained unchanged, whereas it followed the aforementioned trends when g_{Ca} and g_K were held constant.

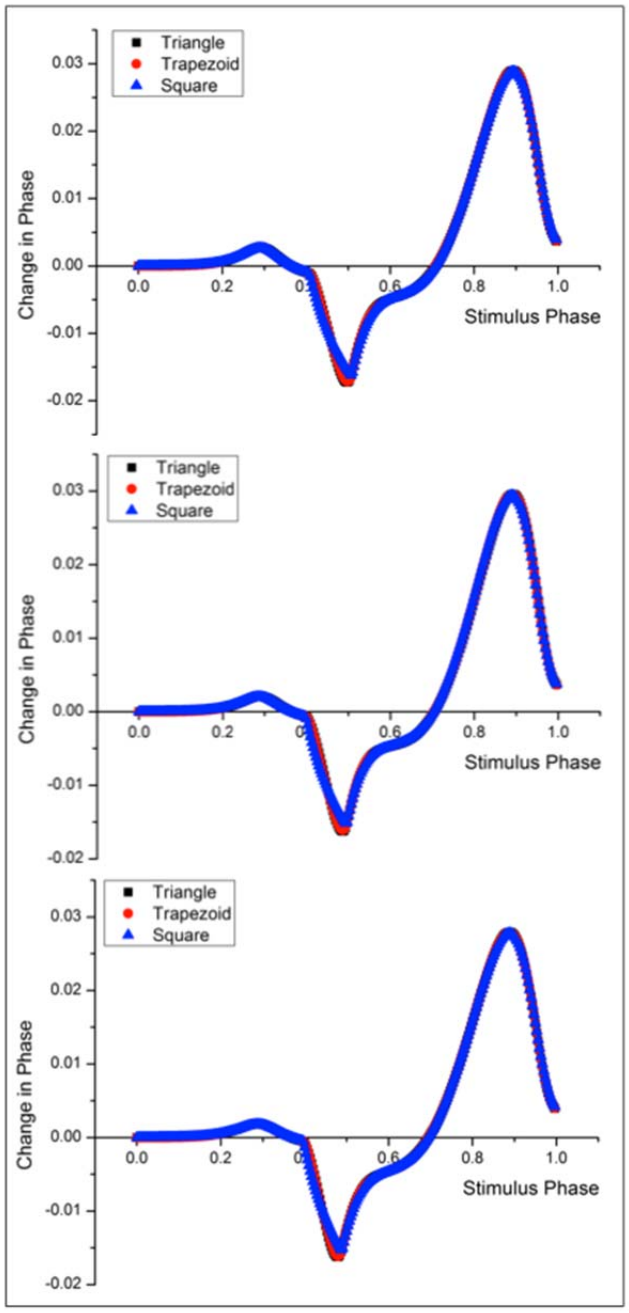

Figure 6. PRCs generated for three model neurons using a rectangular pulse of 10% amplitude, a trapezoidal pulse of 15% amplitude, and a triangular pulse of 20% amplitude, showing how the overall shape of the PRC remains largely unchanged with different external perturbations of the same area.

2. Variable Perturbation Shape

As previously discussed in the Experimental Procedure subsection, we considered rectangular pulse with amplitude of 10% of the injected current, trapezoidal pulse with a 15% amplitude, and triangular pulse with a 20% amplitude. This resulted in a total of 228 individual sets of n^{th} order DSTs. It is already known that changes in perturbation area impact the size and shape of the PRC [11], therefore this method of PRC generation controlled for these changes while allowing any changes caused by perturbation shape to remain expressed in the PRC.

When the shape of the external perturbation was changed, while holding the area of the perturbation constant, the overall shape remained similar (see Fig. 6). On average, 17% of the DST coefficients deviated significantly, while 83% of all DST coefficients had no significant deviation. Figure 6 shows three sets of PRCs generated using rectangular, triangular, and trapezoidal external perturbations, respectively. The conclusion of these numerical simulations is that the overall shape remains very similar when the perturbation shape is changed while keeping the area constant. This trend held true for all trials, as evidenced in the DST analysis performed.

As opposed to changes in the conductance values discussed in the previous subsection, changes in external perturbation shape did not cause any notable drifts in advancing or delaying areas. Some variability was noted in the areas and maximum values of the delaying section, however these changes did not follow any discernible patterns. The advancing section, on the other hand, remained essentially unchanged throughout the trials. This lack of drift is further demonstrated in the higher percentage of DST coefficients with no significant deviation; that percentage being 80% for variable conductances and 83% for variable perturbation shapes.

Discussion

Overall, neither of the biologically relevant control parameters analyzed in this study caused any significant changes to the shape or behavior of the PRC of a Type II ML model oscillator. This was evidenced both in the DST analysis of all the PRCs generated as well as in a graphical analysis of multiple PRCs generated from each group in each trial. This would indicate that the primary factor that impacts the PRC for an individual neuron is something outside of these two parameters, such as the area of the external perturbation or the intrinsic period of the oscillating neuron.

However, the most notable trend discovered was the one between the individual conductance values and the areas of the advancing and delaying functions (see Fig. 5). Although the overall changes in area were relatively small, 6% of the average area at most, this could indicate how neuronal behavior within a larger network is "fine-tuned."

Calcium and leak conductances appeared to perform the same functions, i.e., by increasing the advancing area and decreasing the delaying area (see Fig. 4). Potassium conductance did the opposite by decreasing the advancing area and increasing the delaying area. The leak conductance appeared to have a unique impact on the PRC of a model neuron. When leak conductance was held constant, the advancing area remained relatively constant, and would only increase or decrease if leak conductance was varied. This would indicate that the leak channels, more so than the other ion channels, are what control for the finer details of the advancing area.

These trends, while ubiquitously appearing throughout all trials, did not translate directly to any trends in intrinsic period. Initially, it was expected that small increases or decreases in the intrinsic period were causing this change in area, seeing as the perturbation duration was defined as a percentage of the firing period, so slightly longer periods would result in a slightly longer perturbation. However, since these conductance trends did not correlate with any trends in period, it was determined that this was not the case. Therefore, the individual conductance values must be contributing to a mechanism other than the period, which is what caused these minor changes.

These data agree with previously published data regarding the impact of leak conductance on the PRC of a Type II oscillator [1,3]. When studied using a Hodgkin-Huxley model neuron with similar characteristics to a Morris-Lecar model neuron and a complex multicompartment model neuron, changes in leak conductance value had little influence on the overall shape of the PRC. However, similar drifts in the areas of the advancing and delaying sections were noted by manipulating the value for leak conductance, however in this study both the advancing and delaying areas were increased or decreased [15].

The results from the variable area experiments offer further insight into the mechanisms that control the PRC of a neuron. Specifically, it would indicate that the net electric charge is what contributes most strongly to the PRC, while the shape of the perturbation is of little consequence. This would mean that factors such as the speed of dendrite depolarization and repolarization would not impact the firing patterns of a post-synaptic neuron, as long as the net electric charge was unaffected. Similarly, it would mean that a presynaptic Type I neuron, which would create a triangular external perturbation, and a Type II neuron, which would create more of a trapezoidal external perturbation, have the potential to cause the same changes in postsynaptic firing phase, as long as the net electric charge is the same from both neurons.

We also performed both DSTs and DCTs on the PRCs and found that the smallest number of Fourier coefficients that can accurately represent the PRCs are always determined by the DST. A possible explanation for the effectiveness of DST is the fact that Type II PRCs are bimodal [1,3,9,12]. In fact, very close to the onset of oscillatory behavior, the PRC of any Type II neurons is usually described, in the first approximation, by a sine wave with a constant phase shift that is model-dependent [1,3].

Acknowledgements

R.A.R. acknowledges support from the College of Charleston HHMI Undergraduate Science Education Grant (2010 and 2011). This research was funded by the National Science Foundation CAREER award IOS 1054914 to S.A.O.

References

1 Ermentrout, Bard. "Type I Membranes, Phase Resetting Curves, and Synchrony." Neural Computation 8.5 (1996): 979-1001.

2 Folgering, Joost H.A., Reza Sharif-Naeini, Alexandra Dedman, Amanda Patel, Patrick Delmas, and Eric Honor. "Molecular Basis of the Mammalian Pressure-sensitive Ion Channels: Focus on Vascular Mechanotransduction." Progress in Biophysics and Molecular Biology 97.2-3 (2008): 180-95.

3 Galn, Roberto F., G. Bard Ermentrout, and Nathaniel N. Urban. "Efficient Estimation of Phase-Resetting Curves in Real Neurons and Its Significance for Neural-Network Modeling." Physical Review Letters 94.15 (2005).

4 Hodgkin, A., and Huxley, A. "A Quantitative Description of Membrane Current and Its Application to Conduction and Excitation in Nerve." J. Physiol 117 (1952): 500-544.

5 Kandel, Eric R., James H. Schwartz, and Thomas M. Jessell. Principles of Neural Science. New York: McGraw-Hill, Health Professions Division, 2000.

6 Kullmann, Dimitri M., and Stephen G. Waxman. "Neurological Channelopathies: New Insights into Disease Mechanisms and Ion Channel Function." The Journal of Physiology 588.11 (2010): 1823-827.

7 S. A. Martucci, "Symmetric convolution and the discrete sine and cosine transforms," IEEE Trans. Sig. Processing SP-42, 1038-1051 (1994)

8. Morris, C, and Lecar, H. "Voltage Oscillations in the Barnacle Giant Muscle Fiber." Biophysical Journal 35.1 (1981): 193-213.

9 Oprisan, Sorinel A. "A Geometric Approach to Phase Resetting Estimation Based on Mapping Temporal to Geometric Phase." in Phase Response Curves in Neuroscience: Theory, Experiment, and Analysis, Springer Series in Computational Neuroscience, N.W. Schultheiss et al. (eds.) Vol. 6. New York: Springer Science, 2012. 131-62.

10 Oprisan, S.A., A.A. Prinz, and C.C. Canavier. "Phase Resetting and Phase Locking in Hybrid Circuits of One Model and One Biological Neuron." Biophysical Journal 87.4 (2004): 2283-298.

11 Oprisan, S.A, and C.C. Canavier. "Stability Criterion for a Two-neuron Reciprocally Coupled Network Based on the Phase and Burst Resetting Curves." Neurocomputing 65-66 (2005): 733-39.

12 Oprisan, Sorinel Adrian, and Christian Boutan. "Prediction of Entrainment And 1:1 Phase-Locked Modes in Two-Neuron Networks Based on the Phase Resetting Curve Method." International Journal of Neuroscience 118.6 (2008): 867-90.

13 Oprisan S.A.(2012) Existence and Stability Criteria for Phase-Locked Modes in Ring Networks Using Phase-Resetting Curves and Spike Time Resetting Curves, in Phase Response Curves in Neuroscience: Theory, Experiment, and Analysis, Springer Series in Computational Neuroscience, N.W. Schultheiss et al. (eds.) Vol. 6. New York: Springer Science 419-451.

14 Pan, J., Q. Chen, D. Willenbring, K. Yoshida, T. Tillman, OB Kashlan, A. Cohen, XP Kong, Y. Xu, and P. Tang. "Structure of the Pentametric Ligand-gated Ion Channel ELC Cocrystallized with Its Competitive Antagonist Acetylcholine." Nature Communications 3.714 (2012).

15 Perkel, D. H., J. H. Schulman, T. H. Bullock, G. P. Moore, and J. P. Segundo. "Pacemaker Neurons: Effects of Regularly Spaced Synaptic Input." Science 145.3627 (1964): 61-63.

16 Press, WH; Teukolsky, SA; Vetterling, WT; Flannery, BP (2007), "Section 12.4.1. Sine Transform", Numerical Recipes: The Art of Scientific Computing (3rd ed.), New York: Cambridge University Press

17 Rubin, Jonathan E and Terman, David, Geometric singular perturbation analysis of neuronal dynamics. In Handbook of Dynamical Systems (B. Fiedler editor), pp: 93-146, North-Holland 2000.

18 Stiefel, Klaus M., Boris S. Gutkin, and Terrence J. Sejnowski. "The Effects of Cholinergic Neuromodulation on Neuronal Phase-response Curves of Modeled Cortical Neurons." Journal of Computational Neuroscience 26.2 (2009): 289-301.